

# A novel electro-osmotic pump design for nonconducting liquids: theoretical analysis of flow rate–pressure characteristics and stability

Anders Brask, Goran Goranović, Mads Jakob Jensen and Henrik Bruus

MIC—Department of Micro and Nanotechnology, Technical University of Denmark, Ørstedts Plads, Bldg. 345 East, DK-2800 Kgs. Lyngby, Denmark

E-mail: abr@mic.dtu.dk

Received 30 November 2004, in final form 26 January 2005

Published 11 March 2005

Online at [stacks.iop.org/JMM/15/883](http://stacks.iop.org/JMM/15/883)

## Abstract

We present the design and theoretical analysis of a novel electro-osmotic (EO) pump for pumping nonconducting liquids. Such liquids cannot be pumped by conventional EO pumps. The novel type of pump, which we term the two-liquid viscous EO pump, is designed to use a thin layer of conducting pumping liquid driven by electro-osmosis to drag a nonconducting working liquid by viscous forces. Based on computational fluid dynamics, our analysis predicts a characteristic flow rate of the order nL/s/V and a pressure capability of the pump in the hPa/V range depending on, of course, achievable geometries and surface chemistry. The stability of the pump is analyzed in terms of the three instability mechanisms that result from shear-flow effects, electrohydrodynamic interactions and capillary effects. Our linear stability analysis shows that the interface is stabilized by the applied electric field and by the small dimensions of the micropump.

## 1. Introduction

Electro-osmotic (EO) pumps are suitable for microfluidic applications due to their integrability and compatibility with conventional microtechnology, and moreover they can produce a pulse-free flow without containing any moving parts [1–3]. In EO pumps a liquid is pumped by applying an electric field to the Debye layer. This is formed by the ions in the liquid due to electric screening of the immobile charges on the walls of the pump. In order for such a Debye layer to form, the liquid needs to have significant electrical conductivity, i.e., a sufficiently high concentration of dissociated ions. Nonpolar liquids with very low conductivity ( $<10^{-6}$  S m $^{-1}$ ), such as oil, cannot form the necessary double layer and therefore cannot be pumped in this way [4]. However, as analyzed below, this problem is circumvented in our design by introducing a conducting secondary liquid. By presenting our design and the theoretical analysis of it, we hope to inspire experimental groups to test our ideas and fabricate a device.

The paper is organized in the following way. In section 2, we introduce the general concept of the pump and its novel features. In sections 3 and 4, we turn to a particular, realizable pump geometry and analyze it in terms of flow rate–pressure ( $Q$ – $p$ ) characteristics by means of CFD simulations and equivalent circuit theory. Then, in section 5, we assess the stability of the pump by performing a linear stability analysis of the two-liquid interface. Finally, we draw conclusions in section 6.

## 2. General concept

There are two main types of inline EO pumping schemes in use today. In direct EO pumping, [5, 6], electrodes are in direct contact with a conducting buffer. The buffer enables both the driving force in an electric field, and, due to the charge separation at the walls of a channel, also a bulk-liquid motion, the actual electro-osmotic flow.

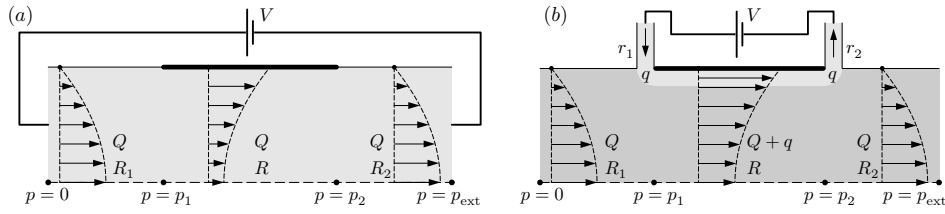


**Figure 1.** (a) The top half of a symmetric channel containing a conducting liquid (light gray), where the EO mobility on the top wall changes step-wise from zero (thin line) in the first section to  $\alpha_{eo}$  (thick line) in the middle section and back to zero (thin line) in the last section. The pressure drops and hydraulic resistances in the three sections are  $0 - p_1$  and  $R_1$ ,  $p_1 - p_2$  and  $R$ , and  $p_2 - p_{ext}$  and  $R_2$ , respectively. The flow profile is shown in each of the sections. (b) A nonconducting working liquid (dark gray) of flow rate  $Q$  flowing through the three-section channel of panel (a), but in addition a conducting pumping liquid (light gray) of flow rate  $q$  enters and exits from two side-channels with hydraulic resistances  $r_1$  and  $r_2$ . In both panels are shown the applied voltage  $V$  that generates the EO flow. The symmetry plane is indicated by the dashed horizontal line in the bottom.

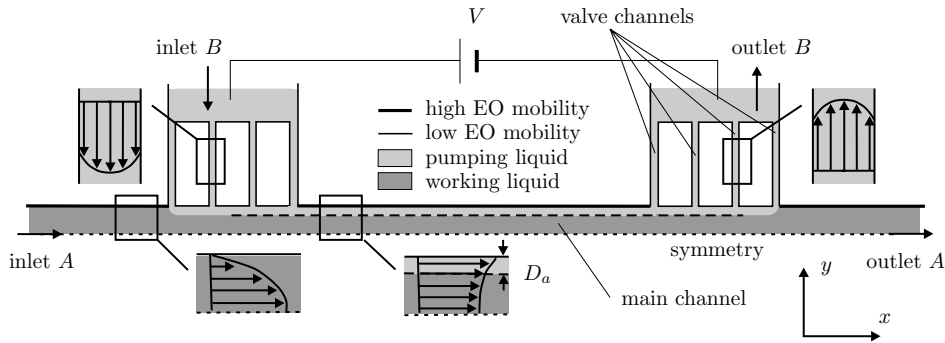


**Figure 2.** Top view of a possible design of the two-liquid viscous pump. The nonconducting working liquid (dark gray) is being dragged by the EO-driven pumping liquid (light gray) that flows along the edge of the main channel. The pump is mirror-symmetric around the central vertical plane, and only one half is shown. The following specific parameters are chosen to predict the performance of the pump. The displayed microchannels are all  $40 \mu\text{m}$  deep. The main channel where the working liquid flows is  $150 \mu\text{m}$  long and  $10 \mu\text{m}$  wide. The narrow valve channels are  $1 \mu\text{m}$  wide and  $42 \mu\text{m}$  long. The un-coated walls are marked as the thick edges of the main channel. Coated walls are marked with thin edges. In inlet A and outlet A the flow is parabolic, while in the valves and in the main channel it is a superposition of parabolic and an EO-induced plug flow.

In the so-called indirect EO pumping the liquid in which the electrodes are separated by some barriers from the liquid where the EO flow takes place. The barriers allow ions but not bulk liquid to pass from the electrode chamber to the EO flow region. The barriers between the two regions can be achieved in several ways. (i) A channel filled with a conducting gel with a large hydrodynamic resistance [2]. (ii) An ion-exchange membrane allowing only positive or negative ions to pass [3]. (iii) A nanometer-sized gap (to allow for the Debye layer overlap) in which bulk EO flow can be suppressed allowing practically only flow of ions [7]. Common for these separation methods is that they are based on the Donnan exclusion principle.

Our novel two-liquid viscous pump can be regarded as a hybrid of the two types of EO pumping. There is still a direct contact between the driving and the bulk layers but they now originate from two different liquids. EO flow is used indirectly as it drives layers of conducting secondary liquids, introduced from some side-channels, to pump a nonconducting liquid through the main channel by viscous forces, see figure 1. Such an arrangement, resembling a conveyor belt, allows the pump to be conveniently positioned anywhere within a microfluidic circuit. To our knowledge it is the only EO pumping mechanism that enables inline pumping of nonconducting liquids. In the following subsections we highlight general principles for the operation of the pump:

pressure valves, under-pressure induced by spatial variations in EO mobility and optimized potential drop. These principles are sketched in figure 2.

### 2.1. Ideal EO flow and pressure valves

In the case of an infinitely thin Debye layer the EO flow rate in a rectangular microchannel of length  $L$ , height  $D$ , and width  $a$  is given by

$$Q_{eo} = u_{eo} Da = \alpha_{eo} V_{eff} \frac{Da}{L} \propto a. \quad (1)$$

Here  $u_{eo}$  is the electro-osmotic velocity,  $\alpha_{eo}$  is the electro-osmotic mobility and  $V_{eff}$  is the electric potential drop inside the channel. We refer to this situation as ideal EO flow. The associated EO pressure  $p_{eo}$  is given by

$$\Delta p_{eo} = Q_{eo} R_{hyd} = \alpha_{eo} V_{eff} \frac{aD}{L} R_{hyd}. \quad (2)$$

For high aspect ratios  $D \gg a$ , the hydraulic resistance is

$$R_{hyd} = \frac{12\mu L}{a^3 D} \frac{1}{1 - 0.63 \frac{a}{D}}, \quad (3)$$

where  $\mu$  is the dynamic viscosity. The pressure-driven flow rate  $Q_p$  through the channel is given by

$$Q_p = \frac{\Delta p}{R_{hyd}} \propto a^3, \quad (4)$$

where  $\Delta p$  is the pressure drop along the channel.

From equations (1) and (4) it follows that the pressure-driven flow will be negligible compared to the EO flow for small values of  $a$ . This can be used to obtain a kind of pressure valves in the two-liquid viscous pump: if narrow channels are placed on the sides of the main channel, their large hydraulic resistance prevents a significant loss of the pressure from the pump into the sides, while at the same time allows the driving EO flow to pass through them. The pressure valves offer two additional advantages. The electrode reservoirs separated by the valves can be exposed to atmospheric pressure. Thus bubble formation from electrolysis will not enter the pump and cause problems. Furthermore, this allows for placing the pump anywhere in a fluidic network.

## 2.2. Under-pressure due to changes in EO flow rate

In order for a nonconducting liquid to enter the pump an under-pressure needs to be induced at the entrance of the pump. This can be achieved by allowing for spatial variation in the EO flow rate  $Q_{eo}$ . Mass conservation ensures that the total flow rate  $Q = Q_{eo} + Q_p$  is constant, so a change in  $Q_{eo}$  implies a change in  $Q_p$  and hence a change in pressure. The change in  $Q_{eo}$  can be obtained either by variations in the EO mobility or by variations in the channel width  $a$  large enough to induce a varying degree of the Debye layer overlap. In this paper we will focus on the first method.

The EO flow given in equation (1) corresponds to a constant EO mobility, in which case no under-pressure is generated inside the channel. If, however, the EO mobility is allowed to change along the channel, a more complex pressure field is obtained. To simplify the discussion without losing the main physics, we study the three-section channel shown in figure 1(a), where the EO mobility changes from zero to  $\alpha_{eo}$  and back to zero. It is the inhomogeneity of the EO mobility that is important, not its specific functional form. The hydraulic resistances of the three sections are  $R_1$ ,  $R$  and  $R_2$ , respectively. The pressure changes from 0 to  $p_1$ , from  $p_1$  to  $p_2$ , and from  $p_2$  to  $p_{ext}$  along the first, second and third section, respectively. Thus the EO pump is set up to work against an external backpressure  $p_{ext}$ . The expressions for the total constant flow rate  $Q$  in each of the three sections are

$$Q = \frac{(0 - p_1)}{R_1} = \frac{(p_1 - p_2)}{R} + Q_{eo} = \frac{(p_2 - p_{ext})}{R_2}. \quad (5)$$

By straightforward algebra this yields

$$Q = \frac{RQ_{eo} - p_{ext}}{R_1 + R + R_2}, \quad (6)$$

$$p_1 = \frac{R_1}{R_1 + R + R_2}(p_{ext} - RQ_{eo}), \quad (7)$$

implying that a positive flow rate will be induced once  $RQ_{eo}$  is larger than the backpressure  $p_{ext}$ . Moreover, an under-pressure  $p_1$  is induced over the first section of the pump, which ensures that liquid is sucked into the pump.

In figure 1(b) this principle of generating an under-pressure is applied to the two-liquid viscous pump. We study the case of immiscible liquids with a stable interface pinned at the corners of the side-channels. In this case the individual flow rates of the pumping and working liquids are constant. For the sake of simplicity we neglect the curvature effects due

to surface tension and postpone this study until sections 4.1 and 5.

The nonconducting working liquid (dark gray) enters the first section of the large, three-section main channel of the hydraulic resistance  $R_1$  and leaves the section of the hydraulic resistance  $R_2$  with the same flow rate  $Q$  given by

$$\frac{1}{R_1}(0 - p_1) = Q, \quad \frac{1}{R_2}(p_2 - p_{ext}) = Q. \quad (8)$$

The conducting pumping liquid (light gray) enters with the flow rate  $q$  through the inlet side-channel having the hydraulic resistance  $r_1$ , and exits with the same flow rate  $q$  through the outlet side-channel having the hydraulic resistance  $r_2$ . Since we are neglecting the Young–Laplace pressure drops from the curved interfaces the pressures  $p_1$  and  $p_2$  are as above, and the flow rate  $q$  is seen to be

$$\frac{1}{r_1}(0 - p_1) = q, \quad \frac{1}{r_2}(p_2 - 0) = q. \quad (9)$$

In the active part of the pump, the middle section with the hydraulic resistance  $R$ , the expression for the total flow rate is simplified, if we assume that the two liquids have the same viscosity (this assumption is easily relaxed in numerical simulations):

$$\frac{1}{R}(p_1 - p_2) + Q_{eo} = Q + q. \quad (10)$$

The expressions for  $Q$ ,  $p_1$  and  $q$  become

$$Q = \frac{RQ_{eo} - p_{ext}}{R_1 + (1 + \frac{R_1}{r_1})R + R_2}, \quad (11)$$

$$p_1 = -R_1Q, \quad (12)$$

$$q = \frac{R_1}{r_1}Q. \quad (13)$$

Like for the simple channel equation (6), a positive flow rate  $Q$  appears once  $RQ_{eo} > p_{ext}$ , and in this case an under-pressure  $p_1$  is generated thus making it possible to suck the nonconducting working liquid into the EO pump. A simulation of the induced under-pressure in the regions below the pressure valves is shown in section 4. In the limit of very high resistance of the side-channel,  $r_1 \gg R_1$ , equation (11) reduces to equation (6). Note, that because we have neglected the Young–Laplace pressure drops, and assumed a stable interface, the external pressure is fixed to be  $p_{ext} = [R_1(r_2/r_1) - R_2]Q$ . Once the full dynamics of the free interface is introduced, the interfaces will adjust its shape to a given  $p_{ext}$ , see section 4.1.

As mentioned, a favorable under-pressure can also be achieved for constant EO mobility by reducing the cross section of the valve region compared to the main channel if the reduction is so large that the Debye layer overlap occurs. The overlap will reduce the EO velocity in the valves and change the flow profile from a plug-like to a parabolic-like one [8]. Since typically the Debye layers are 1–100 nm wide, the pressure valves in this case consist of nanochannels. Depending on the fabrication techniques, the nanochannels can be realized as channels with very high aspect ratio [9], very shallow channels [4], or as parts of nanoporous frits [10].

Regardless of the pump realization, the flow profiles will have some common characteristics. Due to the induced pressures the valve regions and the inlet/outlet regions of the

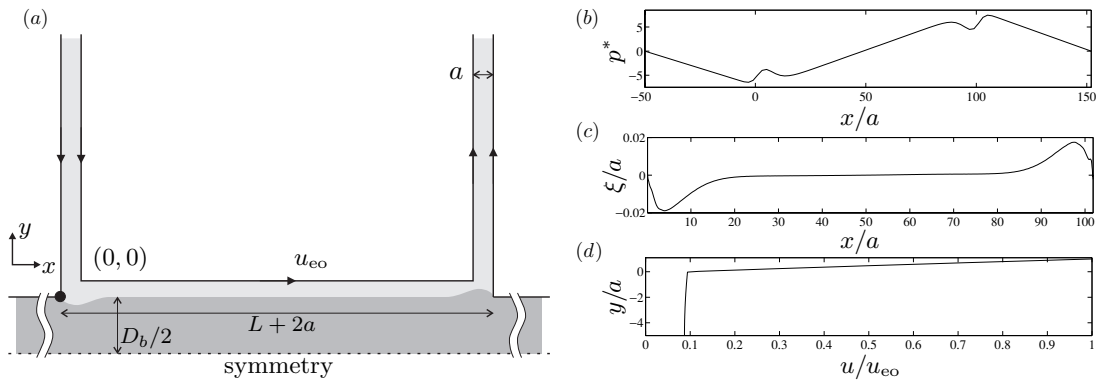


**Figure 3.** (a) The geometry used in the simulation of the immiscible case, where edges with arrows indicate an EO slip velocity  $u_{eo} = 2\text{ mm s}^{-1}$ , (b) The pressure  $p = p^* \mu_{\text{cond}} u_{eo}/a$ , (c) the interface position  $\xi$  and (d) velocity profile across the channel. Viscosities are  $\mu_{\text{cond}} = 1.0 \times 10^{-3} \text{ Pa s}$  and  $\mu_{\text{noncond}} = 300 \times \mu_{\text{cond}}$ . The pressure is plotted along the symmetry axis. The deflection of interface is multiplied by a factor 100 for the purpose of visualization. The velocity profile is taken along  $x = L/2 + a$ .

main channel of the pump will have parabolic flow profiles. In the active part of the main channel the resulting flow is a superposition of an EO flow and an adverse pressure-driven flow, the latter resulting from the mass conservation given in equation (10). Schematic flow profiles are shown in figures 1(b) and 2, while a simulated one is shown in figure 3.

### 2.3. Optimized potential drop

A larger potential drop is needed in the main channel of the pump as compared to the valves in order to generate a higher pressure, equation (2). A single narrow valve channel has a large flow resistance but also a large electrical resistance. This means that the main potential drop would occur in the valve channels and thus not contribute to any pressure build up. The electrical resistance is inversely proportional to the area of the cross section. So, by making many short and narrow channels a low electrical resistance and high hydraulic resistance is obtained. However if the potential drop in the main channel is too large, it could cause instabilities of the two-liquid interface, see section 5.

### 2.4. Priming of the pump

In order for the pump to work an initial positioning of the liquid streams must be taken care of. This is termed as priming of the pump. The priming could happen in different ways depending on the viscosities, surface tensions and the surrounding fluidic network. One way of doing it would be to apply a pressure-driven flow to the side-channels  $q$  and the main channel  $Q$  simultaneously. This would generate a stream of focused nonconducting liquid along the main channel. If the driving pressures are then relaxed at the same time, the interface moves to the pinning points on the side-channels. Computer simulations or experiments may suggest other methods.

## 3. An example of a possible realization

A possible realization with realistic length scales of the two-liquid viscous pump is shown in figure 2. Two sets of four narrow channels are introduced from each side of the main channel as pressure valves. In figure 2 only one side with

inlet/outlet valves is shown, since the device is symmetric around the center plane. Reactive ion etching systems can deliver narrow and deep channels with the aspect ratio as high as 40. So if a valve channel is  $1 \mu\text{m}$  wide it can be  $40 \mu\text{m}$  deep. The overall hydraulic resistance of the valves, equation (3), is 26 times larger than that of the EO section.

The Reynolds number is  $Re \sim 0.01$  and in this creeping flow regime inertia can be neglected. A characteristic feature for creeping flow is that it is free of vorticity. This means that the valve channels may be positioned perpendicular to the main channel without generating any eddies. For a more detailed discussion see [11].

The Debye layer is roughly  $10^4$  times smaller than the total width of the main channel so we do not resolve it in the following modeling of the pump. The EO velocity appears simply as a nonzero slip velocity  $u_{eo}$  at the walls. The reduced EO flow in the valves is, therefore, realized by a reduction in the EO mobility as discussed in section 2.2.

## 4. Theoretical and computational analysis

We have analyzed the performance of the pump described in section 3 using computational fluid dynamics (CFD) simulations and equivalent circuit theory.

### 4.1. Computational fluid dynamics

The simulation effort is divided into two parts: (1) simulations with immiscible liquids, simplified geometry, free surface and velocity boundary conditions, and (2) simulations with miscible liquids, full geometry and EO mobility boundary conditions.

The problem depicted in figure 2 is simulated including the full free surface dynamics. The model is based on the FemLab 3.1 FEM solver and an in-house MatLab based free surface code [12]. The model solves the 2D Stokes equation while enforcing the full free surface stress condition including the Young–Laplace contribution to the pressure. As the problem is very complex only two side-channels are considered, in order to reduce computational time, which still ended to be of the order 24 h on a high performance computer. At the

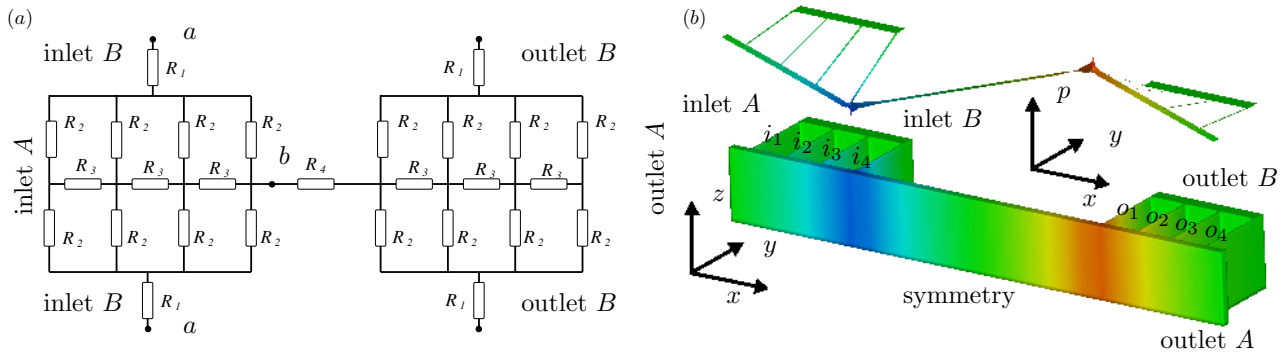


**Figure 4.** (a) The equivalent electric circuit of the two-liquid viscous EO pump. Note that the whole pump/circuit is depicted. The overall resistance is calculated as  $R_{\text{total}} = 2R_{\text{ab}} + R_4$ , where  $R_{\text{ab}}$  is the resistance between node point  $a$  and  $b$ .  $R_4$  is the resistance of the EO section. (b) The calculated pressure distribution inside the pump obtained by numerical simulation in the miscible case with the uniform viscosity  $\mu = 1 \times 10^{-3}$  Pa s. The inset floating above the pump shows how the pressure varies linearly in the main channel between the pressure valves, implying uniform flow. There is no external pressure difference, but note the pressure drop in the pressure valve region ( $i_1 - i_4$ ) which sucks the working liquid into the main channel. Parameters: the dimensions are as in figure 2, while  $\alpha_{\text{eo}}^{\text{low}} = 0.005 \text{ mm}^2 \text{ V}^{-1} \text{ s}^{-1}$ ,  $\alpha_{\text{eo}}^{\text{high}} = 0.05 \text{ mm}^2 \text{ V}^{-1} \text{ s}^{-1}$ ,  $p_{\text{in}} = p_{\text{out}} = 0$ ,  $V = 10$  V. The peak pressure levels are  $p = \pm 10$  Pa.

walls we use velocity boundary conditions to account for the electro-osmotic effects. Figure 3 depicts the simulated geometry with boundary conditions.

The insets (a), (b) and (c) in figure 3 show the dimensionless pressure  $p^*$  along the symmetry axis, the interface position  $\xi$ , and a velocity profile along the vertical symmetry line, respectively. From the results we see that the interface is only slightly deformed and has a thickness comparable to the inlet valve dimensions. The curved shape is a result of the pressure balance including the Young–Laplace pressure. Moreover, we notice that the slip velocity at the interface is about 10% of the wall velocity.

CFD simulations with miscible liquids were made using Coventor 2001.3. The program solves the Laplace equation for the electrical potential and the Navier–Stokes equation for the velocity field. These simulations are complementary to the more complicated free surface simulations. If the pumping liquid is chosen to be water the EO mobility along un-coated walls is typically  $\alpha_{\text{eo}} = 0.05 \text{ mm}^2 \text{ V}^{-1} \text{ s}^{-1}$ . In the valve channels the walls are coated to lower the EO mobility by a factor 10. With these parameters numerical simulations yield a maximal flow rate per volt of  $0.03 \text{ nL s}^{-1} \text{ V}^{-1}$  and a backpressure capacity of  $3 \text{ Pa V}^{-1}$ . The value for the flow rate is specific for the given geometry. According to equations (2) and (3) the backpressure is independent of the length of the pump but strongly dependent on the width of the main channel and the viscosities in the two liquid case. Visualization of the pressure distribution is shown in figure 4(b). Note the under-pressure in the region between valve  $i_1$  and  $i_4$ . The pressure distribution from the immiscible (figure 3(a)) and the miscible case (figure 4(b)) agree qualitatively. Note, that in the miscible case the liquids will mix due to diffusion. Two time scales are involved: (1) the time it takes for the liquid to pass through the pump  $T_{\text{pump}} = L/u_{\text{eo}}$ , (2) and time it takes for the two miscible streams to mix  $T_{\text{diff}} = D_b^2/D$ , where  $D$  is the diffusion constant. The ratio  $T_{\text{pump}}/T_{\text{diff}} = 1.5$  indicates that the liquids will be completely mixed downstream of the pump.

#### 4.2. Equivalent circuit model

The aim is to establish a model that can predict the  $Q$ – $p$  characteristic of the pump. The creeping flow regime allows us to analyze the flow by the equivalent circuit method. We only give an outline here as the detailed procedure is described in [13].

The first step is to find the effective potential drop across the EO section by analyzing the circuit in figure 4(a). In the miscible case with uniform conductivity the result is that 52% of the applied voltage is dropped over the EO section,  $R_4$  in figure 4(a). This value represents a worst case since the main channel is full of conducting liquid leading to a lower voltage drop. In the immiscible case the analysis is complicated by the fact that the resistance  $R_4$  is dependent on the position of the free interface, and an exact result is not obtainable due to lack of computational power. However, our simulations in the two-channel case, section 4.1, indicate that the width of the conducting layer is the same as the width of the side-channels. Since most of the electric field is inside the conducting layer, it is easy to obtain a rough estimate, and we find that 90% of the voltage is dropped over the EO section.

The next step in the equivalent circuit model procedure is to find the hydraulic resistance  $R_{\text{hyd}}$  of each of the channel segments. Since the channel cross sections are all rectangular we make use of equation (3). We then find the backpressure analogous to the treatment in section 2.2.

### 5. Stability analysis

The interface between the two immiscible liquids in the two-liquid viscous pump is generally prone to instabilities. Small perturbations can grow and eventually break-up the surface and disrupt the pumping operation. As sketched in figure 5 there are altogether three types of instability mechanisms at play: shear-flow, electrohydrodynamic and capillary instability. In the following we shall describe and assess the most relevant aspects of each mechanism.

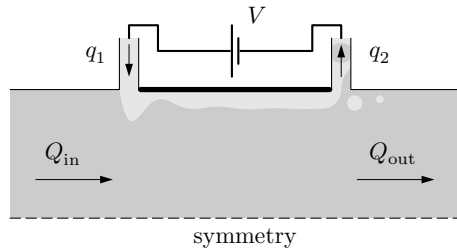


**Figure 5.** A schematic diagram of instabilities in the two-liquid viscous pump. Three main mechanisms of instability are at play: shear-flow and electrohydrodynamic instability are relevant in the main channel and in the outlet valve, while capillary instability plays a role below the valves where the interface curves to compensate for the induced pressures. In the case of break-up of the interphase  $q_1$  and  $q_2$  as well as  $Q_{in}$  and  $Q_{out}$  may differ in contrast to the case of figure 1(b).

### 5.1. Approximations and methods

As long as the conducting layers are thin compared to the nonconducting region, the (in)stability modes on the two interfaces of the symmetric pump from figure 2 will be decoupled from each other. In addition, the symmetric pump can sustain larger adverse pressures known to stabilize the flow [14]. Thus, it suffices to determine the instability window of the simpler asymmetric configuration containing only one interface, i.e., a pump with only one conveyor belt. We further notice that for the high aspect ratio channels under consideration the problem is effectively reduced to two dimensions.

Perturbations of the interface are assumed to be small, and we subject the governing equations and boundary conditions to the usual hydrodynamic linear stability analysis, [15]. The unperturbed interface lies in the  $xy$  plane given by  $z = 0$ . Any slight disturbance of the interface is described as a displacement  $z = \zeta(x, y)$ . We expand all perturbed field  $f$  (velocity  $\mathbf{u}$ , pressure  $p$ , electric potential  $\phi$  and vector  $\mathbf{n}$  normal to the interface) in terms of the small interface position  $\zeta$

$$f = f_0 + \alpha f_1 + \alpha^2 f_2 + \dots, \quad (14)$$

where  $f_0$  represents the unperturbed steady-state solution,  $\alpha$  is the perturbation strength, and  $f_1$  is the first-order solution. Putting the perturbed variables  $f$  into the governing equations and boundary conditions, the steady-state solution cancels out, and by maintaining only terms up to linear order in  $\alpha$  we arrive at the linearized equations which govern the perturbations. The first-order solutions are further expressed in terms of normal modes with the wave vector  $\mathbf{k} = (k_x, k_y)$  and frequency  $\omega_{\mathbf{k}}$

$$f_1(x, y, z, t) = \hat{f}_1(z) \exp[i(k_x x + k_y y) - i\omega_{\mathbf{k}} t]. \quad (15)$$

By inserting the normal modes back into the linearized equations, the problem is eventually transformed into an eigenvalue problem for the frequency  $\omega_{\mathbf{k}}$ , generally a complex number of the form  $\omega_{\mathbf{k}} = \text{Re}(\omega_{\mathbf{k}}) + i \text{Im}(\omega_{\mathbf{k}})$ . It is seen from equation (15) that

$$f_1 \propto \exp[-i \text{Re}(\omega_{\mathbf{k}}) t] \exp[+i \text{Im}(\omega_{\mathbf{k}}) t]. \quad (16)$$

Therefore, an instability (exponential growth in time) is present when  $\text{Im}(\omega_{\mathbf{k}}) > 0$ . In some cases  $\omega_{\mathbf{k}}$  is real for a while before developing a positive imaginary part. In other cases the onset of instability is right at  $\omega_{\mathbf{k}} = 0$ . The former case is known as overstability while the latter as static instability.

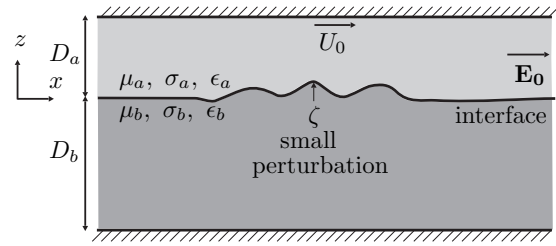


**Figure 6.** The simplified model with a single interface (a single ‘conveyor belt’) used to assess the instability regimes of our pump. Two shearing liquids are confined between two large (high aspect ratio) parallel plates in a Couette–Poiseuille flow. The liquids differ in dynamic viscosities, dielectric constants and conductivities. They are further exposed to a tangential electric field. The Debye layer is assumed negligibly thin so the driving EO velocity appears only as a boundary condition.

### 5.2. Shear-flow instability

Shear-flow instability is particularly relevant in the active part of the main channel, where the liquids are exposed to mutual stresses. Microfluidic shear flows between two viscous, immiscible liquids can result in a variety of regular droplet patterns, as the shear force (constant for a given relative velocity and a fixed geometry) overcomes the cohesive surface tension force, [16].

In our case, due to the conveyor-belt action, the two liquids flow between two large parallel plates in a Couette–Poiseuille setup, figure 6. In each liquid the governing equations are the Navier–Stokes equation and the continuity equation

$$\rho_{(i)} (\partial_t \mathbf{u}_{(i)} + \mathbf{u}_{(i)} \cdot \nabla \mathbf{u}_{(i)}) = -\nabla p_{(i)} + \mu_{(i)} \nabla^2 \mathbf{u}_{(i)}, \quad (17)$$

$$\nabla \cdot \mathbf{u}_{(i)} = 0, \quad (18)$$

where  $i = a, b$  indicates liquid  $a$  and  $b$ ,  $\rho$  is the density,  $p$  is the pressure,  $\mu$  is the dynamic viscosity, and  $\mathbf{u}(x, y, z) = (u, v, w)$  is the velocity field. Note that we did not include the gravitational body force as it is negligible in our microfluidic system<sup>1</sup>.

When the linear stability analysis is performed on equations (17) and (18), we arrive at the Orr–Sommerfeld equations for two liquids, [17], and a set of eight boundary conditions. These include the no-slip velocity conditions at rigid boundaries and fairly complicated interface conditions—continuity of velocities and tangential stresses, and balance of normal stresses. The whole system is then solved for eigenfrequencies as mentioned earlier. The analytical procedure is rather involved. Here we apply the full description, found in [18–21], in the relevant limits.

An important conclusion from the analysis is that a difference between the viscosities of the two liquids cause the instability in shear flows at low Reynolds number. Once the viscosities differ, the relative thickness of the liquid layers becomes important, too.

We have estimated the onset of instability in the long-wavelength limit for the water–oil ( $a$ – $b$ ) system of figure 6. In figure 7  $\text{Im}(\omega_{\mathbf{k}})$  is shown as a function of the viscosity ratio  $\mu_b/\mu_a$ . The graphs are shown for three different thickness

<sup>1</sup> The ratio between gravitational and capillary force in the system is the Bond number,  $Bo = (\rho^{(2)} - \rho^{(1)})ga^2/\gamma$ . If we consider oil and water, and  $a = 10 \mu\text{m}$  is the width of the main channel in the pump, we get  $Bo \sim 10^{-6}$ . This allows the liquids in the pump to flow sidewise.

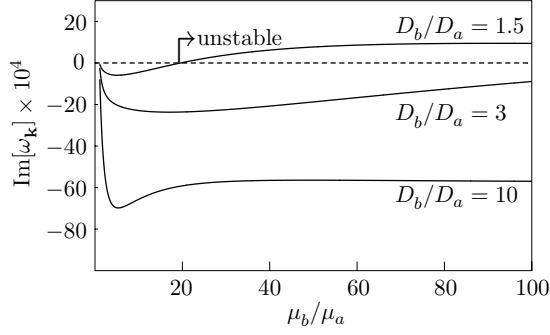


**Figure 7.** A shear-flow stability study of a water–oil system (liquids  $a$  and  $b$ , respectively, in figure 6). For three different values of the thickness ratio  $D_b/D_a$  the imaginary part of the frequency  $\text{Im}[\omega_k]$  is plotted as a function of the viscosity ratio  $\mu_b/\mu_a$  for an EO velocity  $u_{eo} = 1 \text{ mm s}^{-1}$ , a surface tension  $\gamma = 18 \times 10^{-3} \text{ N m}^{-1}$ , and a zero counter-pressure. For  $D_b/D_a = 1.5$ , instability sets in for  $\mu_b/\mu_a > 20$  where  $\text{Im}[\omega_k] > 0$ . This is an example how an increase in viscosity actually enhances instability. Increasing the oil thickness, the window of stability is increased.

ratios  $D_b/D_a$ . Keeping  $D_a$  constant, stability increases with increasing thickness ratio, while it decreases with increasing viscosity ratio, except that in the limit of very large viscosity ratios the system becomes stable again.

The above results can be used to operate the pump within a given stability window. If  $D_a$  is as thin as a few Debye lengths, the pump will practically always be stable with respect to the shear flow.

### 5.3. Electrohydrodynamic (EHD) instability

Another important aspect is electrohydrodynamic (EHD) instability present when liquids of different dielectric constants and conductivities are exposed to electric fields. Numerous studies of EHD instability have been published over the years, e.g. [22–27], and more recently with special attention to microfluidics [18, 19, 28].

In this brief account of EHD instability we use the formalism from [18, 25], and apply it in the relevant limits with regard to our pump. Essentially, the equations governing electric fields and charge transport in each liquid need to be added to equations (17) and (18)

$$\nabla \cdot (\epsilon_{(i)} \mathbf{E}_{(i)}) = \rho_{(i)}^{\text{el}}, \quad (19)$$

$$\nabla \times \mathbf{E}_{(i)} = 0, \quad (20)$$

$$\nabla \cdot (\sigma_{(i)} \mathbf{E}_{(i)} + \rho_{(i)}^{\text{el}} \mathbf{v}_{(i)}) + \partial_t \rho_{(i)}^{\text{el}} = 0, \quad (21)$$

where  $\epsilon$  is the dielectric constant,  $\sigma$  is the conductivity,  $\rho^{\text{el}}$  is the free charge density and  $\mathbf{E}$  is the electric field in each liquid. In equations (19)–(21) it is assumed that magnetic effects are negligible and that Ohm’s law of conduction is valid. The interface boundary conditions are expanded to account for electric stresses and conservation of free charge.

There are two main effects which influence the behavior of the interface between two liquids in an electric field. First, there are polarization forces that act normally on the interface, due to a difference in the dielectric constants. And second, there are tangential shear forces resulting from the free charges that relax at the interface, due to a difference in the conductivities. Relevant in microfluidics are effects involving

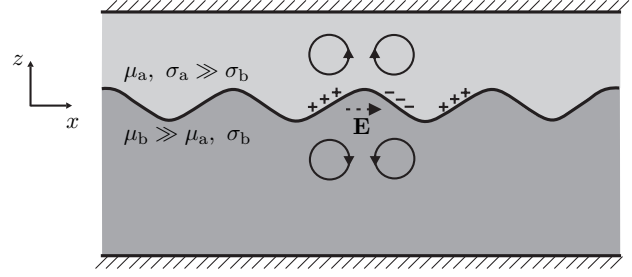


**Figure 8.** Overstability mechanism in the pump. A perturbation of the interface between a conducting and a nonconducting liquid results in the accumulation of free surface charge. As it screens the imposed field from the conducting region, the charge is shifted in phase with respect to the perturbation [25]. Charge motion in a tangential field induces shear stresses in the liquids above and below, which can either stabilize or further destabilize the interface. In the depicted case  $\mu_b \gg \mu_a$  and  $\sigma_a \gg \sigma_b \approx 0$ , so the interface will be stabilized.

Debye layers, but these are out of the scope of this preliminary account.

In our pump a thin layer of conducting liquid drags a viscous nonconducting dielectric liquid. There is a huge difference in conductivities and the liquids are exposed to a tangential electric field. Therefore, the shear forces due to free charges will play the most important role, possibly causing overstability or oscillatory instability, which we now assess.

In equilibrium no current passes through the unperturbed interface and no free charges accumulate on it. However, interface perturbations cause a change in the fields which in turn attract free charges at the interface. The charges position themselves to shield out the imposed field from the high conductivity region. As the charges move under the influence of electric field, shear stresses are passed onto the liquids below and above the interface, creating fluid cells, figure 8. If the liquids have the same viscosity these effects will cancel each other, but a difference in viscosities will make these cells to further deform or possibly suppress the perturbations.

We now make a use of the general eigenvalue solution (equation (34) in [25]) applicable to our problem sketched in figure 6. In the two-liquid viscous pump the two liquids are such that the conductivities  $\sigma_a \gg \sigma_b$  which results in a very short charge relaxation time  $\tau = (\epsilon_a + \epsilon_b)/\sigma_a$ . We are interested in the viscosity limit  $\mu_a \ll \mu_b$ , i.e., when the more conducting liquid is much less viscous. An involved analysis gives for the critical field that induces overstability

$$E_c^2 = -\frac{2\mu_b\sigma_a}{\epsilon_b(\epsilon_a + 3\epsilon_b)}. \quad (22)$$

The minus sign indicates that in this limit no field can induce the instability. In light of figure 8, the imparted viscous stresses, pronounced in the more viscous liquid, act to suppress the interface deformation. On the other hand, if the conducting liquid is the one with a much higher viscosity (e.g. pumping of a gas), the critical field is positive and given by

$$E_c^2 = \frac{2\mu_a\sigma_a}{\epsilon_b(\epsilon_b + 3\epsilon_a)}, \quad (23)$$

or, for  $\epsilon_a \gg \epsilon_b$ ,

$$E_c = \left( \frac{2\mu_a\sigma_a}{3\epsilon_a\epsilon_b} \right)^{\frac{1}{2}}. \quad (24)$$

When equation (24) is evaluated for common fluids, the fields are on the order of  $10^6 \text{ V m}^{-1}$ . In the studied example (operating voltage 10 V), the electric field within the main channel is  $E = 4 \times 10^4 \text{ V m}^{-1}$ , a much lower value.

The above results show that our viscous liquid pump is stable with respect to the EHD overstability. In the case when a more viscous, nonconducting liquid is pumped, stability is always present whereas in the case of low-viscosity dielectrics the critical fields are much higher than the operating ones. In passing we remark that the normal polarization forces also stabilize the interface when the liquid of higher conductivity has also a higher dielectric constant, which is usually the case.

#### 5.4. Capillary instability

The pressure drop over the interface between two immiscible fluids is given by the Laplace equation

$$\Delta P = \gamma \left( \frac{1}{r_1} + \frac{1}{r_2} \right), \quad (25)$$

where  $\gamma$  is the surface tension while  $r_1$  and  $r_2$  are the principal radii of curvature. We take the width  $a$  and depth  $D$  of a valve channel to correspond to  $2r_1$  and  $2r_2$ , respectively. In a high aspect ratio valve  $a \ll D$ , hence only the width  $a$  contributes to the capillary pressure.

The pressure induced below the valves in the two-liquid pump will tend to deform the interface according to equation (25), as simulated in figure 3(c). We now estimate under which conditions the breaking of two streams sketched in figure 5 could occur and why. For an oil–water interface  $\gamma = 18 \times 10^{-3} \text{ N m}^{-1}$  and a valve width of  $a = 1 \mu\text{m}$  it takes a pressure of 36 kPa to push an oil droplet through the valve opening.

The backpressure capacity of the pump is  $\Delta p = 30 \text{ Pa}$  for 10 V using a conducting liquid. In the case of the water–oil interface the pressure increases to  $9 \text{ kPa} \times 0.1 = 900 \text{ Pa}$  at 10 V due to the higher viscosity of oil ( $\mu_{\text{oil}} = 300\mu_{\text{water}}$ ) and the reduced oil velocity, see figure 3(d). This value is still lower than the capillary pressure thus the interface will be stable in normal operation.

If the interphase breaks due to instabilities, e.g., in the case of lower surface tension, oil droplets may enter the outlet valve to account for the mass conservation ( $q_1 \neq q_2$ ). Hence the pinched-off conducting droplets shown in figure 5. Similar effects of variable flow resistance on droplet break-up is demonstrated in [29]. Obviously, such behavior would eventually disrupt the pumping operation.

We conclude this section by saying that the pressure valves will prevent an immiscible liquid from entering them if the backpressure capacity of the pump is smaller than the capillary pressure associated with the valve openings.

## 6. Conclusion

We have presented a novel electro-osmotic pump which can be used to pump nonconducting liquids by the viscous drag of a conducting secondary liquid. In order to achieve a

viable pump, the liquids must be immiscible, stability must be ensured and three main features need to be employed: a favorable under-pressure, pressure valves and an optimized potential drop.

The flow rate–pressure characteristic of the two-liquid viscous EO pump largely depends on the geometrical factors and can be significantly enhanced by advanced etching techniques. The pump design still works for miscible liquids, but here the working liquid gets mixed with the pumping liquid due to diffusion.

Numerical simulations and the equivalent circuit model of the design presented here yield a maximal flow rate per volt of  $0.03 \text{ nL V}^{-1} \text{ s}^{-1}$  and a backpressure capacity per volt of  $3\text{--}90 \text{ Pa V}^{-1}$  depending on the liquids in the pump. These values are quite small and the pump is therefore suited for precise flow manipulation rather than pumping bulk volumes.

Three effects play a role with regard to the stability of the pump: (1) shear-flow instability happens only when the liquids differ in viscosities and is suppressed when the conducting-liquid layer is thin compared to the nonconducting one. (2) Electrohydrodynamic overstability is suppressed when the conducting liquid has a much smaller viscosity than the nonconducting liquid. (3) Capillary instability is suppressed by a large surface tension and by a large value of the capillary pressure stemming from a small width of the pressure valves.

Future work involves time-dependent two-phase simulations. Such work could give valuable information about priming of the pump. We are currently preparing papers containing the detailed mathematical analysis of the stability mechanisms [19, 20]. Finally a prototype should be manufactured. Because of the possibility of pumping all types of liquids in a precise and controlled manner, the described concept and design appear promising.

## Acknowledgments

This work is partly supported by the Danish Technical Research Council,  $\mu\text{TAS}$  Frame Program Grant No. 26-00-0220.

## References

- [1] Laser D J and Santiago J G 2004 A review of micropumps *J. Micromech. Microeng.* **14** R35–R64
- [2] Takamura Y, Onoda H, Inokuchi H, Adachi S, Oki A and Horiike Y 2001 *Proc.  $\mu\text{TAS}$  2001 (Monterey CA, USA, Oct.)* pp 230–2
- [3] Morf W E, Guenat O T and de Rooij N F 2001 *Sensors Actuators B* **72** 266
- [4] Chen C H and Santiago J G 2002 *J. Microelectromech. Syst.* **11** 672–83
- [5] Yao S, Mikkelsen J C and Santiago J G 2001 *Proc. IMECE: ASME International Mechanical Engineering Congress and Exposition (New York, Nov.)*
- [6] Zeng S, Chen C H, Mikkelsen J C and Santiago J G 2001 *Sensors Actuators B* **79** 107–14
- [7] Alarie J P, Jacobson S C, Scott Broyles B, McKnight T E, Culbertson C T and Ramsey J M 2001 *Proc.  $\mu\text{TAS}'01$  (Monterey, CA, USA, Oct.)* pp 131–2
- [8] Levine S, Marriott J R and Robinson K 1974 *J. Chem. Soc. Faraday Trans.* **II** 1–11
- [9] Mogensen K B, Eriksson F, Nikolajsen R P H and Kutter J P 2004 *Proc.  $\mu\text{TAS}'04$  (Malmö, Sweden, Sept.)* vol 1 pp 39–41

- [10] Brask A, Bruus H and Kutter J P 2004 *Proc.  $\mu$ TAS'04 (Malmö, Sweden, Sept.)* vol 2 pp 136–8
- [11] Patankar N A and Hu H H 1998 *Anal. Chem.* **70** 1870–81
- [12] Jensen M J, Garstecki P, Fuerstman M, Bruus H, Whitesides G M and Stone H A 2004 *Proc.  $\mu$ TAS'04 (Malmö, Sweden, Sept.)* vol 1 pp 626–8
- [13] Brask A, Goranović G and Bruus H 2003 *Sensors Actuators B* **92** 127–32
- [14] White F M 1991 *Viscous Fluid Flow* 2nd edn (Singapore: McGraw-Hill)
- [15] Chandrasekhar S 1961 *Hydrodynamic and Hydromagnetic Stability* (Oxford: Oxford University Press)
- [16] Thorsen T, Roberts R W, Arnold F H and Quake S 2001 *Phys. Rev. Lett.* **86** 4163–6
- [17] Drazin P G and Reid W H 1991 *Hydrodynamic Instability* (Cambridge: Cambridge University Press)
- [18] Goranović G 2003 *PhD Thesis* Technical University of Denmark online at <http://www.mic.dtu.dk/research/MIFTS>
- [19] Goranović G, Sørensen M P, Brøns M and Bruus H 2004 *Proc.  $\mu$ TAS'04 (Malmö, Sweden, Sept.)* vol 1 pp 617–9
- [20] Goranović G, Sørensen M P, Brøns M and Bruus H 2004 in preparation
- [21] Yih C-S 1967 *J. Fluid. Mech.* **27** 337–52
- [22] Rayleigh Lord 1882 *Phil. Mag. Ser.* **5** 184–6
- [23] Melcher J R 1963 *Field-Coupled Surface Waves: a Comparative Study of Surface-Coupled Electrohydrodynamic and Magneto-hydrodynamic Waves* (Cambridge MA: MIT Press)
- [24] Melcher J R and Smith C V Jr 1969 *Phys. Fluids* **12** 778–90
- [25] Melcher J R and Schwarz W J Jr 1968 *Phys. Fluids* **11** 2604–16
- [26] Saville D A 1997 *Annu. Rev. Fluid Mech.* **29** 27–64
- [27] Mestel A J 1994 *J. Fluid Mech.* **274** 93–113
- [28] Lin H, Storey B D, Oddy M H, Chen C-H and Santiago J G 2004 *Phys. Fluids* **16** 1922–35
- [29] Link D R, Anna S L, Weitz D A and Stone H A 2004 *Phys. Rev. Lett.* **92** 54503